applied sciences

MDPI

Article

RETRACTED: A Si-αTCP Scaffold for Biomedical Applications: An Experimental Study Using the Rabbit Tibia Model

Piedad N. De Aza [1,*], Miguel A. Rodríguez [2], Sergio A. Gehrke [3], José E. Maté-Sánchez de Val [4] and Jose L. Calvo-Guirado [4]

1 Instituto de Bioingenieria, Universidad Miguel Hernandez, Avda. Ferrocarril s/n 032[illegible]-Elche, Alicante, Spain
2 Instituto de Cerámica y Vidrio, ICV-CSIC, C/Kelsen 5, 28049 Madrid, Spain; ma[illegible]csic.es
3 Biotecnos Research Center, Rua Dr. Bonazo nº 57 Santa Maria (RS), 97015-001 Brasil, sergio.gehrke@hotmail.com
4 Cátedra Internacional de Investigación en Odontología, Universidad C[illegible]lica San Antonio [illegible] Mur[illegible]a, Avda. Jerónimos, 135, Guadalupe, 30107 Murcia, Spain; jemate@uca[illegible].edu [illegible].M.-S.d.V.); jlcalvo@ucam.edu (J.L.C.-G.)
* Correspondence: piedad@umh.es; Tel.:+34-966658485

Received: 5 June 2017; Accepted: 6 July 2017; Published: 8 Ju[illegible]y 2017; Retracted: 27 Octo[illegible]r 2023

Abstract: We herein hypothesize that bioceramic[illegible] with an appropriate architecture made of Si-αtricalcium phosphate (Si-αTCP) meet the biocom[illegible]patibility and bi[illegible]logical safety requirements for bone grafting applications. Polyurethane sponges [illegible]e used as t[illegible]mplates, soaked with ceramic slurry at different ratios and sintered at [illegible]400 °C for 3 h a[illegible].g and cooling rates of 5 °C/min. Four critical size defects of 6 mm Ø we[illegible]e [illegible]ed in 15 NZ tibias. Three working times were established as 15, 30 and 60 days. A highl[illegible] poro[illegible]s [illegible]TCP scaffold with micro and macropores and pore interconnectivity was produced b[illegible] th[illegible]e polym[illegible]r replication method. Considerably more bone formation took place i[illegible]pores and t[illegible]e periphery of the implant for the Si-αTCP scaffolds than for the control grou[illegible]. The ce[illegible]mic scaffol[illegible] (68.32% ± 1.21) generated higher bone-to-implant contact (BIC) percenta[illegible]alues (higher quality, closer contact) than the control group, according to the histomorph[illegible]metric [illegible]lysis, a[illegible]ect closure was significant compared with the control group. The high[illegible]st percentages [illegible] BIC and bone formation were found after 60 days of implantation. These results su[illegible]est that the Si-α[illegible]CP scaffold is advantageous for initial bone regeneration.

Keywo[illegible]ds: polymer [illegible]lication method; porous bioceramics; tricalcium phosphate; in vivo response; tiss[illegible]e reaction; biocomp[illegible]bility

1. Introd[illegible]tion

The feat[illegible]es of the new generation of tissue engineering scaffolds for bone regeneration purposes include being degradable, highly bioactive and mechanically strong [1,2]. Among the many essential factors for tissue engineering scaffolds, macroporous morphology and bioactive composition are assumed to be critical for impacting cell response [3–6].

There are three polymorphs of tricalcium phosphate (TCP): the low-temperature βTCP and the high-temperature forms α and α′TCP. This last form lacks practical interest because it only exists at temperatures ≥1430 °C and reverts almost instantaneously to αTCP on cooling below the transition temperature. In contrast, βTCP is stable at room temperature and transforms reconstructively [7,8] at ≥1125 °C to αTCP, which can be retained during cooling to room temperature [9].

α- and βTCP are currently used in several clinical applications in dentistry, maxillofacial surgery and orthopaedics: βTCP is a component in several commercial mono or biphasic bioceramics and

composites and αTCP is the major constituent of the powder component of various hydraulic bone cements [9–12]. In spite of having the same chemical composition, α- and βTCP differ considerably in their structure, density and solubility, which in turn determine their biological properties and clinical applications.

From a biological point of view, αTCP is non-toxic, osteoconductive and bioactive, both in vitro and in vivo. The main reason for the growing interest in αTCP as a bone implant material is its biodegradability. It is more bioreabsorbable than hydroxyapataie (HA), βTCP and biphasic (HA/βTCP) bioceramics currently used in clinical practice. This makes αTCP an ideal implant material which is able to be replaced by new bone faster than the other calcium–phosphate-based materials currently available on the market.

One of our recent works involved synthesizing a new form of αTCP doped with dicalcium silicate (C_2S) bioceramic powders in the silicocarnotite-tricalcium phosphate subsystem [13] and additionally prepared dense αTCP doped ceramic discs by solid-state processing [14]. One of our former studies has reported the exceptional carbo-hydroxyapatite mineralization ability of αTCP doped ceramic discs in simulated body fluids [15,16]. The released Ca, Si and P, which contained the ionic products from α-TCP doped ceramic, greatly promoted osteogenic differentiation of human mesenchymal stem cells [17,18]. Mate-Sanchez et al. found that Si-TCP grafts displayed greater dimensional stability and better bone to implant contact (BIC) at a % reabsorption rate of ~71.5% of α-TCP and ~42.2% of Si-TCP at day 60 of implantation [19–21]. What these findings indicate is that the chemical composition of Si-αTCP bioceramics is key to enhancing the in vivo behavior of TCP implants.

However, to date, studies on Si-αTCP bioceramics have worked with ceramic discs; hence, none have reported on the fabrication and properties of three-dimensional (3-D) scaffolds. Developing porous Si-αTCP scaffolds to be used as carriers for bone tissue development or as specific release vehicles is therefore of much interest.

Three-dimensional scaffolds for bone tissue engineering are subject to many interrelated biological and structural requirements which must be taken into consideration when selecting the suitable biomaterial for fabrication. An ideal bone tissue scaffold should possess an interconnected porous structure; i.e., it should be highly permeable, with a porosity of >90% and pore diameters in the range 10–500 μm for cell seeding, tissue ingrowth and vascularization, as well as for nutrient delivery and waste removal [22–27]. A particular design criterion of tissue engineering scaffolds is the mimicry and implementation of the bimodal porosity of cancellous bone tissue, which is an important factor for effective scaffold vascularization and for bone ingrowth [28]. Microporosity (≈2–10 μm, <50 μm) is essential for intermediate protein and cell adhesion, cell migration and osteointegration [23,24,27]. Higher pore sizes (>100 μm) are required for enhanced new bone formation, greater bone ingrowth and the formation of capillaries [22,23,25,29,30].

In this study, we applied a polymer replication method [22,31–33] to prepare Si-α-TCP scaffolds with a highly controlled macro and micro structure and pore interconnectivity and we investigated how their pore morphology affected their osteoconductivity and resorption process in vivo for the first time.

2. Materials and Methods

2.1. Preparation and Characterization of the Si-TCP Scaffolds

Dicalcium silicate and tricalcium ceramic powder were synthetized in our laboratory, according to the previously-described processing [8,10].

The dicalcium silicate and tricalcium phosphate in a 3:97 weight % ratio were crushed into dust in an attrition-mill with isopropilic alcohol as liquid medium and ZrO_2-Y_2O_3 balls (1 mm in diameter) for a total of 5 h. A ceramic slurry was prepared with 70% solid contents with a ceramic particle size of 2.1 μm (Mastersizer, Malvern, PA, USA) in a water media. We used 4 weight % of binder (Optapix

PAF-35—Zschimmer Schwartz, Germany) and 2 weight % of defloculant (Dolapix CE-64—Zschimmer Schwartz, Germany). The powder/water ratio was 65:35.

Polyurethane sponges with open cells measuring 60 ppi (BULPREN S. Eurofoam GmbH. Wiesbaden, Germany) were used as templates, soaked with ceramic slurry and sintered at 1400 °C for 3 h at heating and cooling rates of 5 °C/min. Then power was turned off and samples were allowed to cool inside the furnace for 24 h. The final scaffolds had a diameter of 6 mm and a length of 5 mm.

Crystalline phases present in the raw ceramics and in the sintered Si-TCP scaffolds were identified by X-ray diffraction (XRD, Bruker-AXS D8Advance, Karlsruhe, Germany) with a step size of 0.02° at a scanning rate of $10° \cdot min^{-1}$ within the 2θ range of 10–50°, and were observed by scanning electron microscopy (SEM) (Hitachi S-3500N, Ibaraki, Japan) at an accelerating voltage of 20 kV. The pore distribution, pore area, average pore diameter and porosity of the prepared scaffolds were tested by mercury intrusion porosimetry (Quantachrome, Boynton Beach, FL, USA).). The mechanical properties of the scaffolds were measured by the Brazilian test or by the Diametrical Compression of Discs Test (DCDT). Circular discs of a diameter (D) of ~16.60 mm and a thickness (t) of ~5.00 mm (t/D ~ 0.30) were placed between two stainless steel loading plates with their faces perpendicular to the loading plates in a universal testing machine (Model AME-5kN, technical industrial Oawaldo, Prazola Ltda, Guarulhos, Brazil). A load was applied at the displacing rate of the machine's frame of 0.5 mm/min and was applied until the scaffold cracked. The results of 10 valid tests were used to calculate diametrical strength by the procedure of ISO 14801 [34].

2.2. Animals and Surgical Procedure

The Animal Ethics Committee of the Miguel Hernandez University approved the study protocol, which followed Spanish Government and European Community Guidelines for animal care (authorized No. 2014/VSC/PEA/0005 (1032)). The study used 15 male New Zealand rabbits that weighed 3.5–4.5 kg. The Si-TCP scaffold was implanted into two circular critical-size defects (6 mm Ø, 5 mm long) in the animals' tibiae. The total sample size was 15 rabbits with two defects in each tibia, a total of 60 defects, divided randomly into two groups of 30: a test group (Si-TCP scaffold) and a control group (randomization). The surgical procedure and the animals sacrificed were previously reported by our group [11–14].

2.3. Histological and Histomorphometric Analysis

After 15, 30 and 60 days, the implants, together with the surrounding tissues, were removed and fixed in 10% neutral buffered formalin and decalcified. The decalcification method utilized Osteomoll (Merck KGaA, Darmstadt, Germany) containing HCl (10%) and CH_2O (4%), immersing samples for 17 days and renewing the solution every 24 h. The decalcified samples were cleaned and dehydrated in a series of graded ethanol solutions and were embedded in paraffin. The regions that contained implants were cut into 5-µm thick sections with a rotary microtome (Microm HM 340E. Waldorf, Germany) and were stained using hematoxylin-eosin.

The standardized nomenclature of the American Society of Bone and Mineral Research was used for histomorphometric evaluations using Image J software (developed by the National Institute of Health, Bethesda, MD, USA). The entire circumference of each section (containing bone, implant and connective tissue) was traced manually to create an individual region of interest (ROI). Histomorphometric evaluations consisted of measurements of the area of implant material in relation to the total area of interest. Reabsorption was calculated, setting the perimeter area of biomaterial at the baseline and, after the period of analysis, the comparison between them resulted in a resorption rate which was measured as a percentage. The established ROI area was around the perimeter of the biomaterial at the beginning and end of the study period. Examinations were done under a Nikon Elipse 80i microscope (Teknooptik AB, Huddinge, Sweden) equipped with the Easy Image 2000 system (Teknooptik AB), which used 10× to 40× lenses for descriptive evaluations and morphometric measurements. Images were generated with a Leica Z6 APO microscope connected to a Leica DC 500

(Leica, Barcelona, Spain) digital camera, enlarged 23×. After calibrating the system and digitalizing images, interactive measurements of the individual regions of interest (ROIs) were obtained by Leica QWin V3 image analysis software (Barcelona, Spain). The histomorphometric analysis produced one BIC measurement, measured as the percentage of the circumference and length of the cylinder that came into contact with new bone. In the same way, the cortical bone defect in the control group was also evaluated.

The scaffold's resorption rate was determined by an Image J image analysis program (National Institutes of Health, Bethesda, MD, USA), measuring the perimeter of the scaffold after implantation and comparing it with the residual scaffold after 15, 30 and 60 days.

To evaluate the continuing effect of Si-α-TCP scaffold implants from an ultrastructural point of view, cross-sections of the non-decalcified tissues were examined in scanning electron microscopy-energy-dispersive X-ray spectroscopy (SEM-EDS) according to the previously reported SEM protocol [12–14].

2.4. Statistical Analysis

The statistical analysis was performed with PASW Statistics 20.0.0 software (SPSS Inc., Chicago, IL, USA). Sample size was pre-calculated using the statistical method provided by the software. Values were recorded as means ± standard deviation and medians. A pre-statistical analysis of sample distribution was performed to evaluate normality. A non-parametric Wilcoxon test for related samples was applied to compare the means by assuming a 95% level of significance ($p < 0.05$).

3. Results

3.1. Implant Characterization

The polymer replication method enabled the reproduction of highly porous Si-αTCP scaffolds (Figure 1A). Pore diameters that fell within the 300 µm–1.0 mm range and a pore wall thickness of ~60 µm were revealed in the SEM observations (Figure 1B), as were micropores from 1 to 15 µm on struts and pore walls (Figure 1C). A quantitative analysis by EDS was run at different sample points, which determined that scaffold composition was around 0.29 wt % SiO_2, 54.26 wt % CaO and 45.49% P_2O_5. The fact that the apparent density was 70 g·cm^{-3} implied a total porosity of 80%. Hg porosimetry (PoreMaster, Quantachrome, Boynton Beach, FL, USA) demonstrated that 15% of pores were bigger than 1 mm, 20% fell within the 1000–100 µm range and all the rest were under 100 µm. This distribution was centered around 12 µm. The strength of the Si-αTCP scaffold was 0.72 MPa.

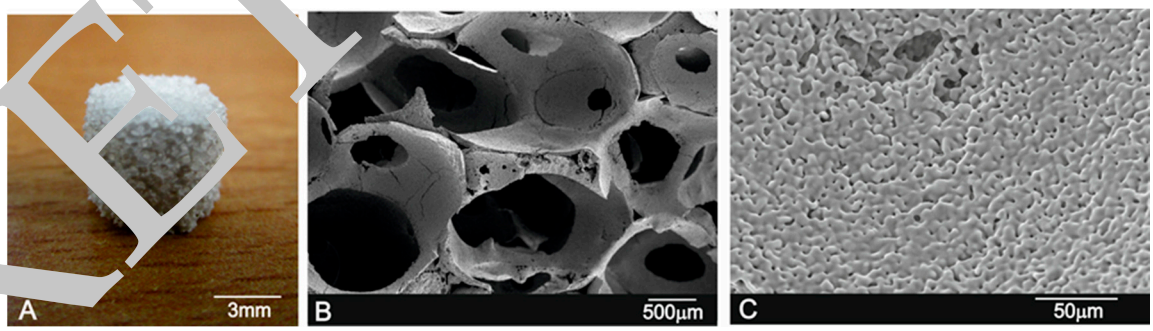

Figure 1. (**A**) Optical image of the Si-αTCP scaffolds obtained by the polymer replication method; (**B**) A low-magnification SEM view of the scaffolds showing interconnectivity and high porosity; (**C**) The high-magnification view of the scaffold reveals a well-distributed microporosity.

The XRD analysis (Figure 2) demonstrates how the prepared scaffolds have a high-temperature metastable α-TCP crystal phase, in spite of the addition of C_2S. The β-TCP to α-TCP transition in TCP took place at 1125 °C [16]. However, the presence of a solid solution of Si in the TCP shifted the

transition temperature to lower temperatures. This solid solution explained the presence of the α–TCP polymorph at room temperature and also explained why the peaks of the JCPD card: 09-0348 and the diffraction peaks of Figure 2 were slightly displaced in the range of 0.1°.

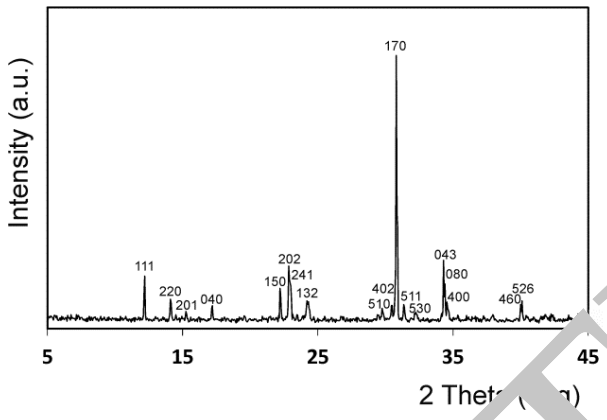

Figure 2. The X-ray diffraction (XRD) pattern of the Si-αTCP scaffolds. All peaks correspond to a high-temperature polymorph of TCP.

3.2. In Vivo Implant Characterization

Figure 3 shows the histological results of the Si-αTCP scaffolds implanted at 15, 30 and 60 days. Not only did all the animals survive the 60-day study period, no evidence of inflammatory cells or fibrous type immediate weaving at the plane of bone neofo was observed.

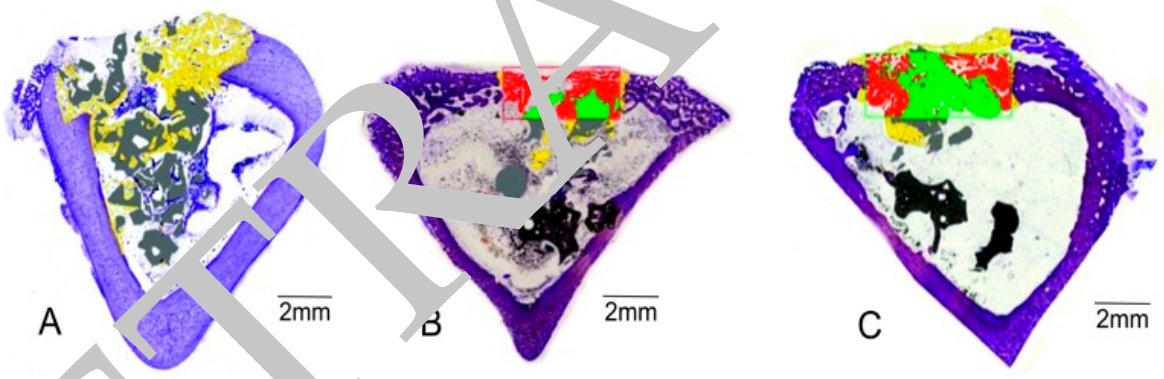

Figure 3. Histomorphometrical analysis of the Si-TCP scaffolds. (**A**) 15; (**B**) 30 and (**C**) 60 days after implantation. Light gray and dark gray areas are residual biomaterial without resorption. The yellow areas correspond to new bone. The regions of interest (ROIs) correspond to the red rectangles. The green color inside the ROI is the biomaterial and the red color is bone. The red color in the middle of the ROI is new bone and the red color in the periphery is old bone. The new bone is thinner than the old one.

In all the samples, woven bone was found in close contact with the scaffold and around it. As expected in rabbit tibial bone, small marrow spaces were noted in the peri-material bone and reached maturity at 15 days as opposed to 60 days. Scaffold volume progressively decreased over the study period. It started with minimal signs at 15 days until the scaffold reabsorbed at 60 days and displayed increased new bone formation at the periphery and within the scaffold pores, which led to it virtually disappearing and a nearly complete cortex closure by day 60. No spontaneous defect closure was noted in the control group, which might be expected of a critical defect. The scaffold samples' resorption pattern presented numerous resorption foci both inside and on the scaffold surfaces, which

generated an irregular pattern. There is an increased bone formation in the medullar zone, together with the remaining scaffold particles surrounded by the new bone.

Bone tissue remodeling was observed in the walls of the control defect at day 60 with abundant blood vessels, but no bone formation in the medullar zone (Figure 4).

Figure 4. Histological analysis of the control group. In (**A**), samples at 15 days after pla ent of the critical defects, the samples showed an intensive granulation reaction in (**B**), samples 30 days, where the bone defect began to be filled by the bone matrix from the bord of the lesion; and in (**C**), 60 days after injury, the defect was closed but the new bone formed was of po quality, mainly in the center of the defect.

The histomorphometric quantification results are shown in Table 1. Analyses were run to determine the scaffold's BIC value and gave high BIC values (68.32 ± 1.21 *). A close contact was noted. New bone ingrowth, connective tissue, defect closure and a residual scaffold were analyzed and recorded and high values were obtained for the implanted scaffold samples.

Table 1. The histomophometric analysis to evaluate the BIC for the Si-TCP scaffold.

	Test Group					Control		
%	15 Days	30 Days	60 Days	Values *	*p* Values **	15 Days	30 Days	60 Days
BIC	54.34 ± 0.32 (54.34)	60 ± 0.13 (33)	.32 ± 1.21 ** (68.32) *	.14	0.038	0.00 ± 0.0	0.00 ± 0.0	0.00 ± 0.0
New Bone	48.83 ± 1.3 (48.83)	52.26 (52.2	(60.11)	0.028	0.011	26.07 ± 0.05 (26.07)	26.26 ± 0.43 * (26.26)	27.10 ± 0.32 ** (27.10) *
Residual	32.1 ± 1.75	29.94 ± 13 (29.94)	23.75 ± 0.85 (23.75)	0.037	0.029	0.00 ± 0.0	0.00 ± 0.0	0.00 ± 0.0
Defect Closure	58.63 ± (58.63)	66.24 ± 4.06 (66.24)	01 ± 94 ** (79.01) *	0.015	0.014	10.87 ± 0.23 (10.87)	25.56 ± 0.43 * (25.56)	28.12 ± 0.32 ** (28.12) *
Reso ate	35.93 ± 0.32 (25.93)	14 ± 1.63 14)	53.13 ± 2.47 (40.13) *	0.023	0.026	0.00 ± 0.0	0.00 ± 0.0	0.00 ± 0.0
Connective Tissue	18.37 ± 1.20 (18.37)	17.3 3.01 (17.30)	16.14 ± 1.33 (16.14)	0.036	0.022	0.00 ± 0.0	0.00 ± 0.0	0.00 ± 0.0

npa ametric Fr dman test. Significant differences $p < 0.05$. Mean ± standard deviation (Median). * Differences b en 15 and 30 ys for each item. ** Differences between 30 and 60 days for each item.

Figure depicts the SEM image of the implant's polished cross-section at 15, 30 and 60 implantation days. The cross-sectional SEM assessment examination showed that all the implants were well integrated into the host tissue and developed an irregular surface caused by their degradation.

After 15 implantation days, newly formed bone tissue covered the whole ceramic implant surface (Figure 5A). The new bone layer comprised Ca-P, largely with traces of Si, given the progressive diffusion of Si ions from the scaffolds to the newly forming bone, which formed part of the biomaterial's resorption process.

A few projections of newly formed bone that reached scaffold particles characterized the bone-to-biomaterial interface (Figure 5B,F). The new bone that filled pores (Figure 5C,F) and loosened

particles (Figure 5D,E) were embedded partly in new bone tissue. In all the samples, bone integration was well advanced and bone penetration had been completed throughout central and deep areas.

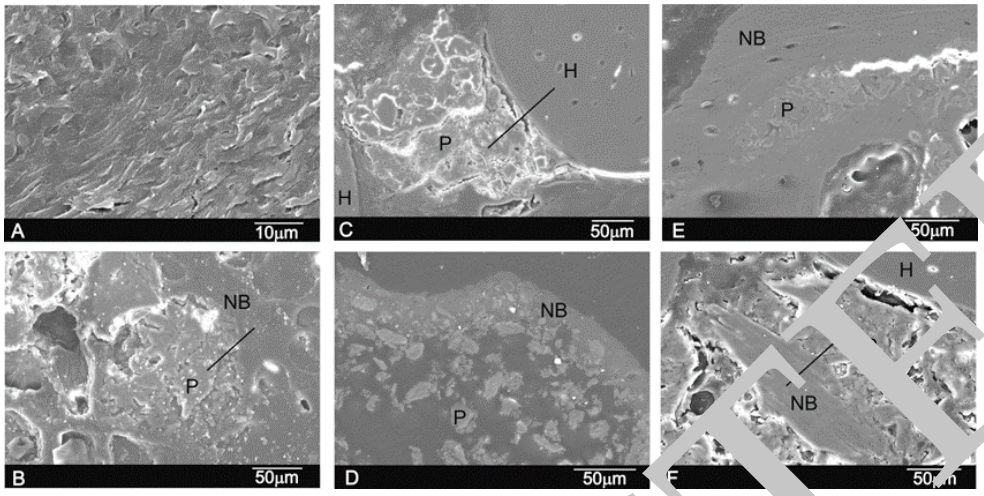

Figure 5. SEM images of the scaffold's cross-section after (**A**,**B**) 15 days (C,D) 30 days and (**E**,**F**) 60 implantation days (H denotes a pore filled with new bone, P refers to implant particles that result from the degradation process, and NB represents new bone tissue).

According to the EDS analysis and the high-magnification SEM examination of the interfaces developed between all the scaffolds and the surrounded [illegible] the reaction zone was characterized by the intermediate presence of the calcium phosphate phase with traces of silica. The EDS analysis was carried out at a series of various points (Figure 5D) and by taking distinct points of interest from the middle to the periphery of the samples to note any changes in the Si/Ca/P ratios. Table 2 offers the descriptive statistics of our database. We saw that the resorption of active biomaterials was underway. The EDS analysis done with the residual scaffold particles in the retrieved tissue gave a Ca/P ratio of varying relative proportions. The elemental analysis of the residual scaffold at different points revealed that the series of particles had distinct mean Ca/P ratios, in accordance with their degradation status. For the statistical data, a relatively high Ca/P ratio was obtained in the residual scaffolds—$1.366 \leq Ca/P \leq 1.74$—and at the bone interface—$2.02 \leq Ca/P \leq 2.34$—according to the elemental analysis and when compared to new bone—$1.81 \leq Ca/P \leq 1.98$. The pre-implantation specific Si ion concentration in the scaffold went from $1.13 \leq Si \leq 1.14$ in the material to a post-implantation ion concentration of $0.07 \leq Si \leq 1.11$, with $0.02 \leq Si \leq 0.05$ at the bone interface versus that of new bone of $0.01 \leq Si \leq 0.02$. What this finding indicates is that the gradual diffusion of the Ca and Si ions from the biomaterial to the newly forming bone at the interface actually formed part of the biomaterial's resorption process.

Table 2. The EDS elemental analysis of the reaction zone at 15, 30 and 60 implantation days. Mean ± SD (median).

(wt %)	O	Ca	P	Si	Ca/P Ratio
Implant/Scaffold					
15 days	44.73 ± 0.12 (44.73)	35.01 ± 0.25 (32.01)	20.25 ± 0.46 (20.25)	0.11 ± 1.62 (0.11)	1.74 ± 0.86 (1.74)
30 days	45.43 ± 0.13 (45.43)	32.12 ± 0.24 (32.14)	22.36 ± 0.43 (22.36)	0.09 ± 1.83 (0.09)	1.44 ± 0.84 (1.[illegible])
60 days	48.47 ± 0.12 (48.47)	29.62 ± 0.26 (29.62)	21.84 ± 0.35 (21.84)	0.07 ± 1.82 (0.07)	1.36 ± 0.76 (1.36)
Bone Interfase					
15 days	50.68 ± 0.11 (50.68)	32.95 ± 0.31 (32.95)	16.32 ± 0.53 (16.32)	0.05 ± 1.63 (0.05)	2.02 ± 0.9[illegible] (2.02)
30 days	55.88 ± 0.10 (55.88)	30.23 ± 0.29 (30.23)	13.85 ± 0.54 (13.85)	0.04 ± 1.33 (0.04)	[illegible] ± 0.84 ([illegible])
60 days	59.15 ± 0.12 (59.15)	28.62 ± 0.32 (28.62)	12.21 ± 0.75 (12.21)	0.02 ± 1.25 (0.02)	2.34 ± 0.96 (2.3[illegible])
New bone					
15 days	59.69 ± 0.15 (59.69)	26.78 ± 0.16 (26.78)	13.5 ± 0.62 (13.50)	0.02 ± 1.63 (0.02)	1.98 ± 0.8[illegible] (1.98)
30 days	60.56 ± 0.09 (60.56)	25.42 ± 0.24 (25.42)	14.01 ± 0.53 (14.01)	0.01 ± 1.[illegible] (0.01)	[illegible] ± 0.91 (1.81)
60 days	63.38 ± 0.09 (63.38)	24.36 ± 0.15 (24.36)	12.25 ± 0.74 (12.25)	0.01 ± [illegible].03 (0.01)	[illegible] ± 0.97 (1.9[illegible])

4. Discussion

A polymer replicated method was followed to prepare the Si-TCP scaffolds [22,31–33]. This method proved most useful as it allowed the simple preparation of highly inter-connective pore structure scaffolds [35,36] within the 1000–300 μm range, which also contained micropores from 1 to 15 μm as well as a high porosity of 80% (Figure 1). The Si-TCP scaffolds' porous properties covered the nutrient transportation and cell/bone tissue ingrowth requirements. Small pores favoured hypoxic conditions and induced osteochondral formation before osteogenesis, while large pores that were well-vascularized lead to direct osteogenesis [22,23,25,29,30].

The material's mechanical behavior also sufficed to handle and place the material inside the surgical site, with a strength of 0.72 MPa. Si-αTCP presented improved mechanical strength compared to the traditional HA (0.03–0.29 MPa) [36], β-TCP (less than 0.1 MPa) [20], 45S5-Bioglass (0.42–0.6 MPa) [37] and CaSiO$_3$ (2.5 MPa) [38] scaffolds prepared by the same method. The mechanical strength obtained for the Si-αTCP scaffolds fell within the same range as that for human sponge bone (0.2–4.0 MPa) [39]. This indicates that the Si-αTCP scaffolds covered the mechanical requirements for handling in vivo and in cell culture implantations for bone tissue engineering applications. As the sintering temperature of Si-αTCP scaffolds can go up to 1400 °C, which is a substantially higher temperature than that of HA scaffolds (1100 °C), βTCP scaffolds (1200 °C) and 45S5 Bioglass (<900 °C), the Si-αTCP's higher sintering temperature can result in dense pore walls and may contribute to improved mechanical strength.

Ionic substitution plays a key role in the biological chemistry of bone apatite, whose crystallographic structure is similar to that of hydroxyapatite ($Ca_5(PO_4)_3OH$). Several anionic ($CO_3^{=}$) and cationic (K, Na, Sr, Mg) substitutions were induced in crystals of bone apatite [40–47]. These ionic substitutions resulted in microscopic crystals, which were not only appropriately insoluble for stability but also adequately reactive to allow the remodeling process of resorption and re-precipitation in vivo. The incorporation of Si ions herein successfully induced the synthesis of the high-temperature form of the TCP ceramic, as the XRD analysis indicated.

We herein tested the bone regeneration capacity of the Si-TCP scaffolds by creating critical bone defects in the tibial bone of rabbits by using empty bone defects as controls.

The Si-αTCP scaffolds' morphological and structural properties resulted in enhanced new-bone formation and a greater degradation than the Si-αTCP dense ceramics [19–21]. The novel Si-TCP scaffolds were superior to the pure TCP dense ceramics in terms of their biological performance in vivo. Si-αTCP promoted significantly better bone formation and a higher degradation rate.

This degradation is compatible with the bone deposition rate because the presence of fibrous tissue was limited. More mature bone in the defects treated with Si-αTCP scaffolds was also observed. The ionic radius of the silicon ions was 0.41 Å, which was a higher radius than that of phosphorus

(0.34 Å). Therefore, the Si-O bond length (0.161) was longer than that of the P-O bond (0.155) and the ionic radius of the phosphate group (PO_4^{3-}) was shorter than that of the silicon group (SiO_4^{4-}) [48–51]. This may diminish the stability of calcium phosphates, thus enhancing their solubility, and may explain the greater degradability observed for the Si-αTCP scaffolds.

The histomorphometric results of the present study obtained a value of 60.11% for the Si-αTCP-treated bone defect, which was filled by newly formed bone by 60 healing days. New bone ingrowth was located in the vicinity of the implant ceramic particles and within the scaffold. This is possibly owing to the scaffold´s open porosity (76%) and crystallinity. High porosity was seen to facilitate the resorption process as the pores´ external and external surface areas were exposed to the medium, which brought about an increase in the calcium and phosphorous ion release—59.0 ± 0.42 (31.57) and 40.52 ± 0.87 (14.10), respectively—into the intercellular medium for several microns beyond the scaffold body.

The new bone ingrowths in the implant were more evident at 30 and 60 days and as the process further entered the implant, they advanced into the spaces between the implant's exposed scaffold particles to form a characteristic interlocking pattern at the interface. The SEM (Figure 5) showed massive bone colonization of the implant through the original scaffold pores caused by the structure's gradual dissolution. These advanced processes implied that the scaffold material's free particles were detected in many areas across the restructuring implant. The fact that the densities inside the material and at the bone-ceramic interface significantly and gradually reduced implied that the restorative process not only went from the periphery to the center, but were initiated in an early material implantation stage by a cellular mechanism [29,30].

5. Conclusions

We successfully prepared bioactive porous Si-αTCP scaffolds with a highly porous large-pore microstructure by way of a polymer replication method.

The porous Si-αTCP scaffolds possessed a high porosity and a large pore size, as well as an improved mechanical strength compared to other β-TCP scaffolds obtained by the same method. Within the limitations of this in vivo rabbit study, it may be stated that the porous Si-αTCP scaffolds are a valid effective alternative to other materials used for bone tissue engineering. The scaffolds underwent dissolution when the ion exchange mechanism took place and they were exposed to the natural environment and were able to transform into a bone-like structure. Thus, they can be fully integrated into natural bone, which functions while they temporarily take over during the implantation process. The porous Si-αTCP scaffolds are a promising implant material candidate in orthopedic, oral and maxillofacial applications given their biological and mechanical properties.

Acknowledgments: Part of this work has been supported by Spanish Ministry of Economy and Competitiveness (MINECO) contract grant numbers: MAT2013-48426-C2-1-R and MAT2013-48426-C2-2-R.

Author Contributions: Miguel A. Rodríguez performed the preparation of the implants by polymer replication method; Piedad Nieves De Aza performed the implant and the SEM post implantation characterization; Sergio A. Gehrke and José E. Maté Sánchez de Val performed the statistical analysis and the histology and histomorphology characterization; Jose L. Calvo Guirado and José E. Maté Sánchez de Val conducted the surgeon. José E. Maté Sánchez de Val and Piedad N. De Aza designed and performed the experiments and prepared the manuscript. Also all the authors contributed to the analyses and discussion of the results.

Conflicts of Interest: The authors declare no conflicts of interest.

References

1. Ros-Tarraga, P.; Mazon, P.; Rodriguez, M.A.; Meseguer-Olmo, L.; De Aza, P.N. Novel resorbable and osteoconductive calcium silicophosphate scaffold induced bone formation. *Materials* **2016**, *9*, 785. [CrossRef]
2. Rabadan-Ros, R.; Velásquez, P.A.; Meseguer-Olmo, L.; De Aza, P.N. Morphological and structural study of a novel porous nurse's a ceramic with osteoconductive properties for tissue engineering. *Materials* **2016**, *9*, 474. [CrossRef]

3. Karageorgiou, V.; Kaplan, D. Porosity of 3D biomaterial scaffolds and osteogenesis. *Biomaterials* **2005**, *26*, 5474–5491. [CrossRef] [PubMed]
4. De Mulder, E.L.W.; Buma, P.; Hannink, G. Anisotropic Porous Biodegradable Scaffolds for Musculoskeletal Tissue Engineering. *Materials* **2009**, *2*, 1674–1696. [CrossRef]
5. Gerhardt, L.C.; Boccaccini, A.R. Bioactive Glass and Glass-Ceramic Scaffolds for Bone Tissue Engineering. *Materials* **2010**, *3*, 3867–3910. [CrossRef]
6. Ros-Tarraga, P.; Rabadan-Ros, R.; Murciano, A.; Meseguer-Olmo, L.; De Aza, P.N. Assessment of Effects of Si-Ca-P Biphasic Ceramic on the Osteogenic Differentiation of a Population of Multipotent Adult Human Stem Cells. *Materials* **2016**, *9*, 969. [CrossRef]
7. Buerger, M.J. *Crystallographic Aspects of Phase Transformations, in Phase Transformations in Solids*; Smoluchowski, R., Meyer, R.J.E., Weyl, W.A., Eds.; John Wiley & Sons Inc.: New York, NY, USA, 1951; pp. 183–211.
8. Elliot, C. *Structure and Chemistry of the Apatites and Other Calcium Orthophosphates*, 2nd ed.; Elsevier Science: Amsterdam, The Netherlands, 1994.
9. Carrodeguas, R.G.; De Aza, S. α-tricalcium phosphate: Synthesis, properties and biological applications. *Acta Biomater.* **2011**, *7*, 3536–3546. [CrossRef] [PubMed]
10. Dorozhkin, S.V. Calcium orthophosphate cements for biomedical application. *J. Mater. Sci.* **2008**, *43*, 3028–3057. [CrossRef]
11. Bohner, M. Calcium orthophosphates in medicine: From ceramics to calcium phosphate cements. *Injury* **2000**, *31* (Suppl. D), 37–47. [CrossRef]
12. Morejón-Alonso, L.; Bareiro, O.J.; Carrodeguas, R.G.; dos Santos, L.A. Bioactive composite bone cement based on α-tricalcium phosphate/tricalcium silicate. *J. Biomed. Mater. Res. Part B Appl. Biomater.* **2012**, *100*, 94–102. [CrossRef] [PubMed]
13. Martinez, I.M.; Velasquez, P.A.; De Aza, P.N. The sub-system α-TCP–Silicocarnotite within the binary system $Ca_3(PO_4)_2$–Ca_2SiO_4. *J. Am. Ceram. Soc.* **2012**, *95*, 1112–1117. [CrossRef]
14. Martinez, I.M.; Velasquez, P.A.; De Aza, P.N. Synthesis and stability of α-tricalcium phosphate doped with dicalcium silicate in the system $Ca_3(PO_4)_2$–Ca_2SiO_4. *Mater. Charact.* **2010**, *61*, 761–767. [CrossRef]
15. Martinez, I.M.; Velasquez, P.A.; Meseguer-Olmo, L.; De Aza, P.N. Production and study of in vitro behaviour of monolithic α-Tricalcium Phosphate based ceramics in the system $Ca_3(PO_4)_2$–Ca_2SiO_4. *Ceram. Int.* **2011**, *37*, 2527–2535. [CrossRef]
16. Martinez, I.M.; Velasquez, P.A.; Meseguer-Olmo, L.; Bernabeu-Esclapez, A.; De Aza, P.N. Preparation and characterization of novel bioactive α-tricalcium Phosphate doped with Dicalcium Silicate ceramics. *Mater. Sci. Eng. C* **2012**, *32*, 876–886. [CrossRef]
17. Meseguer-Olmo, L.; Aznar-Cervantes, S.; Mazón, P.; De Aza, P.N. In vitro behaviour of adult mesenchymal stem cells of human bone marrow origin seeded on a novel bioactive ceramics in the Ca_2SiO_4-$Ca_3(PO_4)_2$ system. *J. Mater. Sci. Mater. Med.* **2012**, *23*, 3003–3014. [CrossRef] [PubMed]
18. Velasquez, P.; Luklinska, Z.B.; Meseguer-Olmo, L.; Mate-Sanchez de Val, J.E.; Delgado-Ruiz, R.A.; Calvo-Guirado, J.L.; Ramirez-Fernandez, M.P.; de Aza, P.N. αTCP ceramic doped with Dicalcium Silicate for bone regeneration applications prepared by powder metallurgy method. In vitro and in vivo studies. *J. Biomed. Mater. Res. A* **2013**, *101*, 1943–1954. [CrossRef] [PubMed]
19. Mate-Sanchez de Val, J.E.; Calvo-Guirado, J.L.; Delgado-Ruiz, R.A.; Ramirez-Fernandez, M.P.; Martinez, I.M.; Granero-Marin, J.M.; Negri, B.; Chiva-Garcia, F.; Martinez-Gonzalez, J.M.; De Aza, P.N. New block graft of α-TCP with silicon in critical size defects in rabbits: Chemical characterization, histological, histomorphometric and micro-CT study. *Ceram. Int.* **2012**, *38*, 1563–1570. [CrossRef]
20. Mate-Sanchez de Val, J.E.; Calvo-Guirado, J.L.; Delgado-Ruiz, R.A.; Ramirez-Fernandez, M.P.; Negri, B.; Abboud, M.; Martinez, I.M.; De Aza, P.N. Physical properties, mechanical behavior, and electron microscopy study of a new α-tcp block graft with silicon in an animal model. *J. Biomed. Mater. Res. A* **2012**, *100*, 3446–3454. [CrossRef] [PubMed]
21. De Aza, P.N.; Luklinska, Z.B.; Mate-Sanchez de Val, J.E.; Calvo-Guirado, J.L. Biodegradation process of α-tricalcium phosphate and α-tricalcium phosphate solid solution bioceramics in vivo: A comparative study. *Microsc. Microanal.* **2013**, *19*, 1350–1357. [CrossRef] [PubMed]
22. Yang, S.; Leong, K.F.; Du, Z.; Chua, C.K. The design of scaffolds for use in tissue engineering. Part I. Traditional factors. *Tissue Eng.* **2001**, *7*, 679–689. [CrossRef] [PubMed]

23. De Aza, A.H.; Velasquez, P.; Alemany, M.I.; Pena, P.; De Aza, P.N. In situ bone-like apatite formation from a Bioeutectic®ceramic in SBF dynamic flow. *J. Am. Ceram. Soc.* **2007**, *90*, 1200–1207. [CrossRef]
24. Rezwan, K.; Chen, Q.Z.; Blaker, J.J.; Boccaccini, A.R. Biodegradable and bioactive porous polymer/inorganic composite scaffolds for bone tissue engineering. *Biomaterials* **2006**, *27*, 3413–3431. [CrossRef] [PubMed]
25. Tabata, Y. Biomaterial technology for tissue engineering applications. *J. R. Soc. Interface* **2009**, *6*, S311–S324. [CrossRef] [PubMed]
26. Santos, M.I.; Reis, R.L. Vascularization in Bone Tissue Engineering: Physiology, Current Strategies, Major Hurdles and Future Challenges. *Macromol. Biosci.* **2010**, *10*, 12–27. [CrossRef] [PubMed]
27. Chiu, L.L.Y.; Radisic, M. Scaffolds with covalently immobilized VEGF and Angiopoietin-1 for vascularization of engineered tissues. *Biomaterials* **2010**, *31*, 226–241. [CrossRef] [PubMed]
28. Smith, I.O.; Ren, F.; Baumann, M.J.; Case, E.D. Confocal laser scanning microscopy as a tool for imaging cancellous bone. *J. Biomed. Mater. Res. B Appl. Biomater.* **2006**, *79*, 185–192. [CrossRef] [PubMed]
29. Temenoff, J.S.; Mikos, A.G. *Biomaterials: The Intersection of Biology and Materials Science*; Pearson International Edition: London, UK, 2008; p. 471.
30. Honda, M.; Fujimi, T.; Izumi, S.; Izawa, K.; Aizawa, M.; Morisue, H. Topographical analysis of proliferation and differentiation of osteoblasts in micro- and macropores of apatite ceramic scaffold. *J. Biomed. Mater. Res. A* **2010**, *94*, 937–944. [CrossRef] [PubMed]
31. Yunos, D.M.; Bretcanu, O.; Boccaccini, A.R. Polymer-bioceramic composites for tissue engineering scaffolds. *J. Mater. Sci.* **2008**, *43*, 4433–4442. [CrossRef]
32. Baino, F.; Ferraris, M.; Bretcanu, O.; Verné, E.; Vitale-Brovarone, C. Optimization of composition, structure and mechanical strength of bioactive 3-D glass-ceramic scaffolds for bone substitution. *J. Biomater. Appl.* **2013**, *27*, 872–890. [CrossRef] [PubMed]
33. Baino, F.; Caddeo, F.S.; Novajra, G.; Vitale-Brovarone, C. Designing porous bioceramic scaffolds to model healthy and osteoporotic bone. *J. Eur. Ceram. Soc.* **2016**, *36*, 2175–2[illegible] [CrossRef]
34. International Organization for Standardization. *ISO 14801—Dentistry—Implants—Dynamic Loading Test for Endosseous Dental Implants*, 3rd ed.; International Organization for Standardization: London, UK, 2016.
35. Hulbert, S.F.; Morrison, S.J.; Klawitter, J.J. Tissue reaction to three ceramics of porous and non-porous structures. *J. Biomed. Mater. Res.* **1972**, *6*, 347–374. [CrossRef] [PubMed]
36. Hollister, S.J.; Maddox, R.D.; Taboas, J.M. Optimal design and fabrication of scaffolds to mimic tissue properties and satisfy biological constraints. *Biomaterials* **2002**, *23*, 4095–4103. [CrossRef]
37. Tadic, D.; Epple, M. Mechanically stable implants of synthetic bone mineral by cold isostatic. *Biomaterials* **2003**, *24*, 4565–457[illegible] [CrossRef]
38. Hench, L.L. The story of Bioglass®. *J. Mater. Sci. Mater. Med.* **2006**, *17*, 967–978. [CrossRef] [PubMed]
39. Carrodeguas, R.G.; de Aza, A.H.; [illegible]ez, J.; de Aza, P.N.; Pena, P.; López-Bravo, A.; de Aza, S. Preparation and in vitro characterization of wollastonite doped tricalcium phosphate bioceramics. *Key Eng. Mater.* **2008**, *361–363*, 237–240. [CrossRef]
40. Bernhardt, K.; Imbert, L.; [illegible]er, C.; Auregan, J.C.; Cruel, M.; Ogier, A. Microscale mechanical and mineral heterogeneity of human cortical bone governs osteoclast activity. *Bone* **2017**, *94*, 42–49. [CrossRef] [PubMed]
41. Carrodeguas, R.G.; De Aza, A.H.; Turrillas, X.; Pena, P.; De Aza, S. New approach to the β→α polimorphic transformation in magnesium-substituted tricalcium phosphate and its practical implications. *J. Am. Ceram. Soc.* **2008**, *91*, 1281–1286. [CrossRef]
42. García [illegible] I.H.; Garcıa Carrodeguas, R.; de Aza, A.H.; Baudin, C.; Pena, P. Effect of Mg and Si co-substitution on microstructure and strength of tricalcium phosphate ceramics. *J. Mech. Behav. Biomed. Mater.* **2014**, *30*, 1–15. [CrossRef] [PubMed]
43. Zilm, M.; Thomson, S.D.; Wei, M.A. Comparative Study of the Sintering Behavior of Pure and Manganese-Substituted Hydroxyapatite. *Materials* **2015**, *8*, 6419–6436. [CrossRef]
44. Pina, S.; Ferreira, J.M.F. Brushite-Forming Mg-, Zn- and Sr-Substituted Bone Cements for Clinical Applications. *Materials* **2010**, *3*, 519–535. [CrossRef]
45. O'Donnell, M.D.; Hill, R.G. Influence of strontium and the importance of glass chemistry and structure when designing bioactive glasses for bone regeneration. *Acta Biomater.* **2010**, *6*, 2382–2385. [CrossRef] [PubMed]
46. Cannillo, V.; Sola, A. Potassium-based composition for a bioactive glass. *Ceram Int.* **2009**, *35*, 3389–3393. [CrossRef]

47. Ros-Tárraga, P.; Murciano, A.; Mazón, P.; Gehrke, S.A.; De Aza, P.N. In vitro behaviour of sol-gel interconnected porous scaffolds of doped wollasonite. *Ceram. Int.* **2017**, *43*, 11034–11038. [CrossRef]
48. Aina, V.; Malavasi, G.; Fiorio Pla, A.; Munaron, L.; Morterra, C. Zinc-containing bioactive glasses: Surface reactivity and behaviour towards endothelial cells. *Acta Biomater.* **2009**, *5*, 1211–1222. [CrossRef] [PubMed]
49. Xu, S.; Lin, K.; Wang, Z.; Chang, J.; Wang, L.; Lu, J. Reconstruction of calvarial defect of rabbits using porous calcium silicate bioactive ceramics. *Biomaterials* **2008**, *29*, 2588–2596. [CrossRef] [PubMed]
50. Serena, S.; Caballero, A.; De Aza, P.N.; Sainz, M.A. New evaluation of the in vitro response of silicocarnotite monophasic material. *Ceram. Int.* **2015**, *41*, 9411–9419. [CrossRef]
51. Lugo, G.J.; Mazón, P.; De Aza, P.N. Phase transitions in single phase Si-Ca-P-based ceramic after thermal treatment. *J. Eur. Ceram. Soc.* **2015**, *35*, 3693–3700. [CrossRef]